*Journal of Earth Science, Online 2017* *ISSN 1674-487X*
*Printed in China*
https://doi.org/10.1007/s12583-017-0943-1

# The Quantitative Measurement of Bedding Orientation Using Remote Sensing Data: Yili Basin, Northwest China

**Zhenghai Wang**[1, 2], **Weilong Lin**[1], **Ruxin Ding**[*1]
1. *School of Earth Science and Engineering, Sun Yat-sen University, Guangzhou, China,* 510275
2. *Guangdong Provincial Key Laboratory of Mineral Resources and Geological Processes, Guangzhou, China,* 510275
Zhenghai Wang: http://orcid.org/0000-0002-4300-3987; Ruxin Ding: http://orcid.org/0000-0002-1174-5193

**ABSTRACT: Bedding orientation measurement is a remote sensing application used in the field of geology, but the results are often unsatisfactory when the bed is dislocated along the strike direction. This paper proposes a new method called Multiple-line Method that is designed to improve bedding orientation measurement. This technique uses the bed as a vector, and fits the vectors as a plane to obtain the bedding orientation. This study employs the case of Yili Basin and measures 25 bedding orientations using the Multiple-point and Multiple-line methods, respectively. The result shows that the errors from the Multiple-line Method are mostly smaller than those from the Multiple-point Method when a bed is discontinuous.**
**KEY WORDS: bedding orientation, Multiple-Line Method, remote sensing, Yili Basin.**

## 0 INTRODUCTION

The application of remote sensing data can drastically increase the efficiency of field reconnaissance, especially in the areas that are difficult to access (Abellán et al., 2006). This developing technology provides large-scale, high-precision, multi-sensor, multi-spectral and multi-temporal images of the Earth's surface, and increases the efficiency of geological information extraction, such as alteration information extraction, bedding orientation measurement, etc..

In the 1960s, the theory of using aerial photo to measure the attitude began to appear and apply, but due to the limitation of the resolution of the remote sensing image and the ability of processing, it didn't popularize (Tator et al., 1960). In the 1990 s, scholars began to try to take advantage of aerial stereo image pair to determine strata occurrence, this kind of method can achieve higher precision, but the costs were too high and processing cycle were very long, so it was not suitable for calculation of a large batch of occurrence (e.g., Chen et al., 1991; Berger et al., 1992). Entering the 21st century, scholars put forward some methods to acquire the occurrence of shallow stratum based on CORONA images, P5 image pair and GeoEye-1, and also some methods to measure the attitude of rock based on 3DGIS (Liu et al., 2000). Berger et al. (1992) tried to understand the feasibility of utilizing the SPOT stereo pair to extract the occurrence of geological planar structure. Chen et al. (1991) achieved the goal of extracting the attitude of rock on the microcomputer automatically by using the linear projection platform to get the quantitative attitude of rock, through the diagram method. Pu et al. (2012) made use of the Google Earth function of artificial point pick, background count and foreground display. Nowadays, the methods to distinguish the attitude of rock have already changed from visual estimation to automatic or semi-automatic extraction.

The multiple-point method has been widely used to measure bedding orientations based on remote sensing images such as the panchromatic and stereo ones acquired by the SPOT and CORONA satellites (Chen et al., 1991; Berger et al., 1992; Bilotti et al., 2000). This method uses selected points to fit a virtual plane, and then calculates the bedding orientation (Berger et al., 1992). However, the fitting accuracy may need to be improved when the bed is dislocated (Fernandez et al., 2009; Dhont et al., 2005; Reif et al., 2011; Pu et al., 2012).

With the recent development of aerospace engineering, satellites have provided a large quantity of images of relatively high resolution that display the outlines of rock outcrops more clearly, which allows more accurate measurements of the earth's surface. In order to utilize the high spatial resolution images to improve the fitting accuracy for discontinuous outcrops, we proposed a new method based on the theory of planar fitting. A certain plane can be fitted by a number of points or lines. Using points leads to the Multiple-point method (Berger et al., 1992), while using lines leads to the method described in this paper. This paper expresses a line as a vector, and fits the vectors to a plane after moving the origins of them to a common point. We therefore named the method Multiple-line method. Using this method, the adjacent beddings are assumed to parallel to each other in a small range, and the vectors from different beddings can be treated as the same source; in this way, the Multiple-line Method can reduce the errors involved with using the Multiple-point Method.

This paper takes the Yili Basin, Xinjiang Province, to exemplify the applications of the multiple-line and the multiple-point

*Corresponding author: dingrux@mail.sysu.edu.cn


Manuscript received Apr 15, 2016.
Manuscript accepted Oct 09, 2016.

method. The results are compared with field data and then discussed to clarify the applicability of the two methods.

## 1 METHODOLOGY

Figure 1 illustrates the principles used in the Multiple-line Method. Plane a represents the ground surface and planes b, c, d stand for the strata, while lines *A–B* and *C–D* are the traces which are the intersections between planes b and d with plane a, and two lines are not parallel in space. Because line *A–B* is recorded as a vector, it can move to line *A'–B'*, and the same is true for lines *C–D* and *C'–D'*. By combining the vectors *A'–B'* and *C'–D'*, we can fit the best plane as plane c, and plane c is parallel to planes b and d.

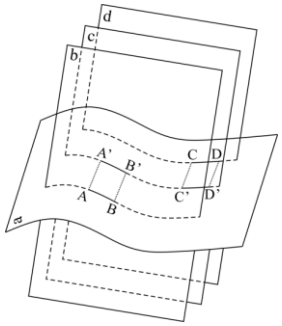


**Figure 1.** Model of the Multiple-line Method. Plane a is the ground surface, planes b and d represent the strata, which intersect the plane a at lines *A–B* and *C–D*. We can fit a plane by moving lines *A–B* and *C–D* to *A'–B'* and *C'–D'*, respectively, and the fitted plane, plane c as shown in the figure, is parallel to planes b and d, so the bedding orientation can be determined.

We classified the situation related to discontinuous traces into three types: flat field, mountain ridge, and mountain slope (Fig. 2). In the model, plane a represents the ground, and planes b and c are the surfaces of strata, which are assumed to be parallel; plane a is cut by a solid trace. We can fit the best planes (i.e., planes b and c) by the Multiple-line Method, but if we mistakenly believe that points A, B and C come from the same plane, and fit the plane with the points using the Multiple-point Method, incorrect points will be selected from different strata leading to an incorrectly fitted plane, represented by plane d (Fig. 2). In the flat field model, the plane fitted by the Multiple-point Method is subhorizontal, with an uncertain dip direction. For the mountain ridge model, the dip of plane d is nearly correct while the dip direction expresses an obvious error. Mountain slopes are relative rare in the real world, and the traces of outcrops are shown as curved lines, which make plane fitting difficult for both of the methodsThe Multiple-point Method depends on fitting the plane using the least sum of squares of the distance from every point to the plane, and then calculates the orientation of the plane. Based on data from the Multiple-lines Method, we express a line in the form of a vector, and recorded it as ($x_i$, $y_i$, $z_i$). Therefore, we can calculate the fitted plane by the vectors, which is expressed as A$x$ + B$y$ + C$z$ + D = 0. Many methods can be used to calculate the bedding orientation of the plane, including planar regression, analysis of moment of inertia, and vector calculus(Fernández 2005; Jones et al.,2009); some improvements are available for each of these methods (Zhou et al., 2011).

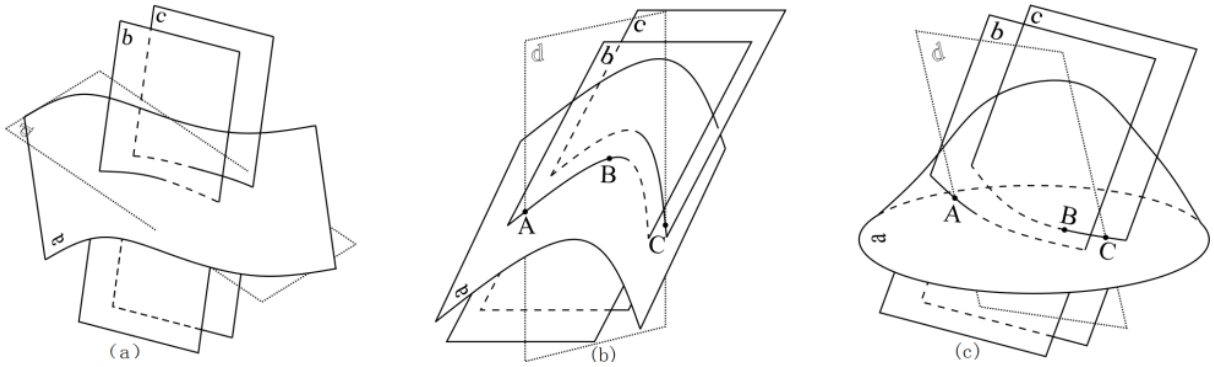


**Figure 2.** Models used in the application of the Multiple-line and Multiple-point methods.In both models, plane a represents the ground; planes b and c represent the strata. The models included (a) a flat field, (b) a mountain ridge and (c) a mountain slope.

In this paper, we used the Least Sum of Squares Method to calculate the best plane. For *n* lines, we can express them as *n* vectors. We suppose the vectors ray from the origin, so *D* in the expression of fitted plane is 0, and the sum of squares of distances from the head of vectors to the fitted plane can be described as:

$$S(x,y,z)=\sum_{i=1}^{n}\left[\frac{|Ax_i+By_i+Cz_i|}{\sqrt{A^2+B^2+C^2}}\right]^2=\sum_{i=1}^{n}\frac{(Ax_i+By_i+Cz_i)^2}{A^2+B^2+C^2}$$

when S(x,y,z) reach its minimum, we can get the best fitted plane. After taking the partial derivatives of the three variables, Eqs. 1 can be changed into:

$$\begin{cases}\sum_{i=1}^{n}x_i(Ax_i+By_i+Cz_i)=0\\ \sum_{i=1}^{n}y_i(Ax_i+By_i+Cz_i)=0\\ \sum_{i=1}^{n}z_i(Ax_i+By_i+Cz_i)=0\end{cases} \quad (2)$$

After solving the equations set, we can calculate the normal vector of plane (A, B, C), and determine the bedding orientation in the next step.

The bedding orientation can be described by two parameters: dip and strike. The strike is the direction (azimuth) of a geological surface, measured clockwise from the true north and ranging between 0 °to 359 °. Dip is the angle (inclination) of a geological surface measured from a horizontal plane (perpendicular to the

strike direction) (Dadon et al., 2011). A former study provided the equations needed to calculate the dip (θ) and strike (φ) (Bilotti et al., 2000; Liu et al., 2011; Chen et al., 2007). In another paper, bedding orientation was recorded as dip (θ) and dip direction (ω). Dip direction was the direction of the horizontal trace of the line of dip, measured clockwise from the true north and also ranging between 0 °to 359 °(Grenon and Laflamme, 2011). For instance, a plane with strike 80 ℃NE and dip 60 ℃NW, could be also described as dip direction 10 ℃NW and dip 60 ℃(Koike *et al*.,2011). The three parameters, dip (θ), strike (φ) and dip direction (ω) can be calculated under certain conditions using Eqs. 3, 4, and 5. This paper uses dip and dip direction to define a plane.

$$\begin{cases} \theta = \cos^{-1}(C/\sqrt{A^2+B^2+C^2}) & C \geq 0 \\ \theta = \cos^{-1}(-C/\sqrt{A^2+B^2+C^2}) & C < 0 \end{cases} \quad (3)$$

$$\begin{cases} \phi = \cos^{-1}(A/\sqrt{A^2+B^2}) & A > 0 \\ \phi = \cos^{-1}(-A/\sqrt{A^2+B^2}) + \pi & A < 0 \end{cases} \quad (4)$$

$$\begin{cases} \omega = \cos^{-1}(B/\sqrt{A^2+B^2}) & A \times C > 0 \\ \omega = \cos^{-1}(B/\sqrt{A^2+B^2}) + \pi & A \times C < 0 \end{cases} \quad (5)$$

Based on the theory of the Multiple-line Method, we determined the bedding orientation by the following steps.

(1) Create a three dimensional view. Drag the remote sensing image onto the digital elevation model (DEM); generate a three dimensional view which allows us to scan the geology in a simulated world. Landsat, ALOS, SPOT, and Quickbird satellite images are usually used as the remote sensing images, and the DEM can be downloaded from the United States Geological Survey website or generated by stereo pair.

(2) Measure the trace of the target outcrop. First, we draw lines to highlight the trace, and measure some necessary parameters of the lines. The parameters can be measured in two ways, the heading and dip, or the different values between the head and tail of the lines. In this step, we record lines as vectors.

(3) Fit the plane by lines. The plane equation can be calculated by Eqs. 2 and the parameters of lines measured above. With Eqs. 3, 4, 5 and normal vector of plane, we calculate the dip, strike and dip direction of the fitted plane, which are the bedding orientations of the target stratum.

## 2 A CASE STUDY IN YILI BASIN

### 2.1 Regional Setting

This paper applied the methods described above to a well-exposed area, located in northwestern China (Fig.3). Our study area (43 ℃15′– 44 ℃15′N, 81 ℃15′–83 ℃15′E) is bordered by the Yili Basin in the west, Awulale Mountain in the east, Keguqin Mountain in the north and Chabuchaer Mountain in the south (Zhou et al., 2011). All these mountains are sparsely vegetated have low population density, and their elevations are above 1 000 m. Structures of the physical geology in this area are mostly east-west-tending, including the Kashenhe Fault between the Keguqin Mountain and Awulale Mountain, the Gongnaisi Fault between the Awulale Mountain and Chabuchaer Mountain and the Moheer Fault between Yili Basin and the Awulale Mountain.

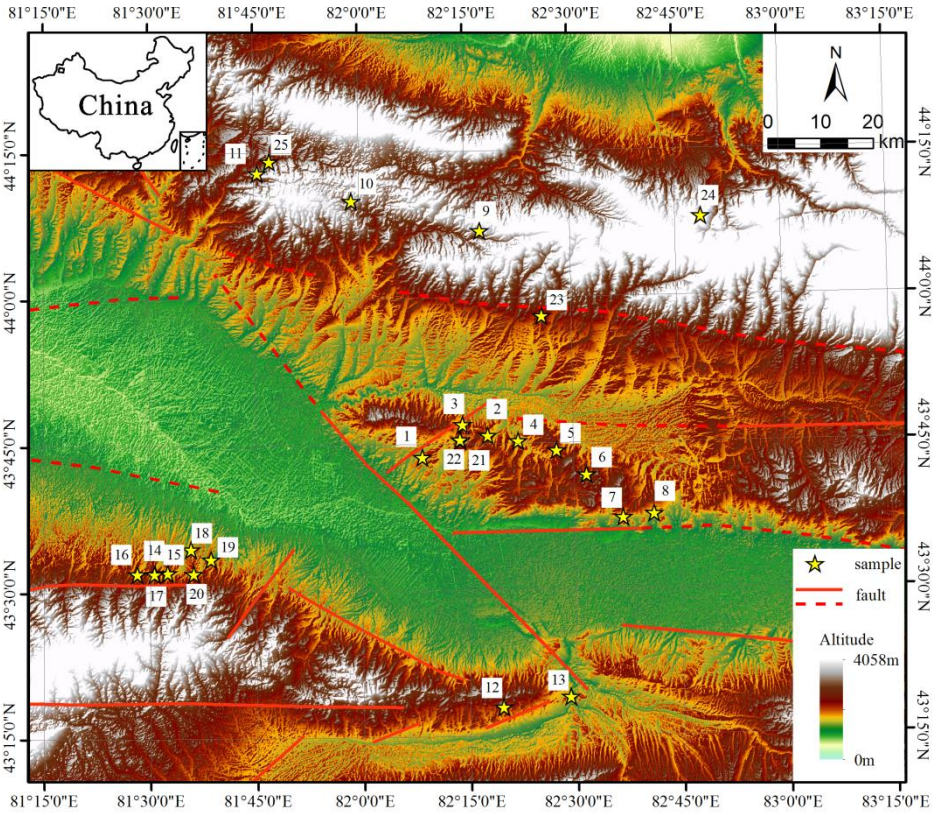


**Figure 3.** Digital elevation model of the study area showing major faults and sampling locations. Solid lines indicate active faults visible at the surface; dash lines indicate concealed faults. Inset map: vicinity showing the study area in northwestern China.

## 2.2 DATA PROCESSING

We selected Google Earth as the experimental platform, which is a basically near-perfect GIS data services platform released in 2005. Google Earth integrates raster and vector data of many kinds, such as a DEM as well as aerial and satellite photos from different companies. Google Earth provides boundary and road data, and we focused on the DEM as well as aerial and satellite photos in our study. The resolution of the DEM in Google Earth is generally less than 100 m, and is 30 m in most parts of China. The images were acquired from many different companies, such as the QuickBird from DigitalGlobe, Landsat-7 from EarthSat and SPOT6 from Astrium. In addition, some aerial images came from BlueSky and Sanborn (Tan and Song, 2011). A former study clipped and mosaicked the QuickBird images from Google Earth, combined that mosaic with the DEM generated from the CORONA stereo images, and measured the bedding orientation for future studies (Chen *et al*., 2009).

Google Earth provided us a desired view by the combination of a DEM and remote sensing images. A schematic diagram was used for the measurement of bedding orientation at Site No. 8 (Fig.4; 43°37'36.11"N, 82°41'44.44"E), which is overlooking a sight at 1680 m in elevation. In this example, a QuickBird remote sensing image provided by Digital Globe was obtained on 28 August 2014 with a resolution of 0.61 m. The DEM was from the Global DEM generated using stereo-pair images collected by the ASTER instrument onboard Terra, with a spatial resolution of about 30 m (1 arc-second). In Fig.4, the green line marks the trace of an outcrop, and the yellow line used as a ruler for measuring. In this example, the yellow line cover 69.37 m on the ground, and its projection on the horizontal plane is 63.53 m. In addition, the heading of this measured line is 84.09°. After measuring more than two lines for each plane, we fitted the plane as well as the bedding orientation by Eqs. 3, 4, and 5.


**Figure 4.** Example of bedding orientation measurement at Site No. 8. Image provided by Google Earth, and generated by dragging the QuickBird image onto the digital elevation model data. Green lines, highlight for bedding traces; yellow line, measured trace.

## 3 RESULTS AND DISCUSSIONS

In this paper, we determined 25 bedding plane orientations by both Multiple-line and Multiple-point methods, and compared them with the field data. Table 1 compares the measured results and the field data, where the dip direction errors and dip errors are represented by the difference in the values of the field data and the results measured by the two methods employed here. In the analyses of dip direction error, a positive value indicates the dip direction determined by one of the two methods that was measured in a clockwise direction when compared with the field data; conversely, a negative value indicates it was measured in a counter clockwise direction. Therefore, the dip direction errors range from −180° to 180°. The dip errors are expressed as the relative error (Table 1). Fig.5 and Fig.6 show the distribution of error intuitively. The blue and brown points represent the errors in data collected using the Multiple-line and Multiple-point method, respectively, for dip direction and data (Fig.5 and Fig.6, respectively). These figures clearly show that the Multiple-point Method has a larger bias than the former. All the dip direction errors from Multiple-line Method data are within 50°while 7 of 25 results exceeded 50° for from Multiple-point Method data. In addition, the mean ± standard errors of the absolute differences between the calculated results and field data are 10.2°±8.6°for Multiple-line Method and 19.0°±18.3°for Multiple-point Method in dip direction (excluding points 6, 11, 15 and 19 for both methods).

As to the errors of dip for both methods, we obtained the relative errors for both methods. The Multiple-line Method was also better than the Multiple-point Method for this type of measurement. Most of the results from Multiple-line Method are closer to 0 when compared with the Multiple-point Method data. Similarly, we count the mean ± standard errors of the absolute difference for dip; the results show that the errors of the Multiple-line Method data were 9.7°±10.2°while errors of the Multiple-point Method data were 16.1°±12.9°.

We classified the errors into two categories: artificial and systemic errors. Artificial errors are mostly determined by the method used to choose the lines. For both the Multiple-line and Multiple-point methods, we can obtain more accurate results by choosing the marked bedding as the fitted vector, taking the measured line with the higher difference in elevation at each side or by setting a longer-stretch measuring line during the operation.

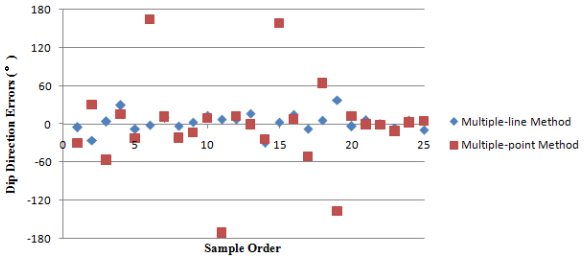


**Figure 5.** Errors of dip direction for the Multiple-line and Multiple-point methods. Positive values indicate the errors are clockwise from the field data while negative values indicate the opposite.


**Figure 6.** Relative errors of dip for the Multiple-line and Multiple-point methods.

**Table1** Comparison between measurement results and field data

| Order | The observed data | | Multiple-line Method | | | | Multiple-point Method | | | |
|---|---|---|---|---|---|---|---|---|---|---|
| | Dip direction (°) | Dip (°) | Dip direction (°) | Dip direction error (°) | Dip (°) | Relative error of dip (%) | Dip direction (°) | Dip direction error (°) | Dip (°) | Relative error of dip (%) |
| 1 | 322 | 38 | 316.84 | -5.16 | 48.74 | 0.28 | 291.97 | 30.03 | 4.93 | -0.87 |
| 2 | 166 | 10 | 140.50 | -25.50 | 12.21 | 0.22 | 196.45 | 30.45 | 27.92 | 1.79 |
| 3 | 175 | 50 | 179.06 | 4.06 | 35.26 | -0.29 | 118.84 | 56.16 | 16.02 | -0.68 |
| 4 | 230 | 10 | 259.64 | 29.64 | 13.03 | 0.30 | 244.72 | 14.72 | 19.13 | 0.91 |
| 5 | 344 | 40 | 336.31 | -7.69 | 32.13 | -0.2 | 321.99 | 22.01 | 46.6 | 0.17 |
| 6 | 331 | 40 | 329.87 | -1.13 | 36.31 | -0.09 | 135.14 | 164.14 | 69.16 | 0.73 |
| 7 | 355 | 80 | 5.11 | 10.11 | 83.12 | 0.04 | 6.24 | 11.24 | 89.82 | 0.12 |
| 8 | 189 | 80 | 186.29 | -2.71 | 71.86 | -0.10 | 167.46 | 21.54 | 51.93 | -0.35 |
| 9 | 206 | 65 | 209.60 | 3.6 | 68.50 | 0.05 | 193.04 | 12.96 | 35.8 | -0.45 |
| 10 | 182 | 40 | 196.02 | 14.02 | 33.89 | -0.15 | 190.84 | 8.84 | 26.78 | -0.33 |
| 11 | 26 | 20 | 33.38 | 7.38 | 16.79 | -0.16 | 215.53 | 170.47 | 15.33 | -0.23 |
| 12 | 299 | 65 | 306.72 | 7.72 | 70.58 | 0.09 | 310.79 | 11.79 | 68.75 | 0.06 |
| 13 | 357 | 50 | 14.11 | 17.11 | 54.66 | 0.09 | 356.60 | 0.40 | 69.96 | 0.40 |
| 14 | 33 | 13 | 3.53 | -29.47 | 8.95 | -0.31 | 9.11 | 23.89 | 9.27 | -0.29 |
| 15 | 356 | 44 | 359.35 | 3.35 | 29.73 | -0.32 | 154.55 | 158.55 | 64.68 | 0.47 |
| 16 | 350 | 65 | 4.78 | 14.78 | 48.01 | -0.26 | 357.65 | 7.65 | 61.41 | -0.06 |
| 17 | 19 | 13 | 11.72 | -7.28 | 8.71 | -0.33 | 327.84 | 51.16 | 29.28 | 1.25 |
| 18 | 157 | 34 | 162.85 | 5.85 | 36.64 | 0.08 | 221.14 | 64.14 | 18.49 | -0.46 |
| 19 | 340 | 14 | 17.28 | 37.28 | 9.61 | -0.31 | 202.8 | 137.2 | 10.48 | -0.25 |
| 20 | 331 | 45 | 327.28 | -3.72 | 42.32 | -0.06 | 342.93 | 11.93 | 72.59 | 0.61 |
| 21 | 178 | 64 | 183.34 | 5.34 | 32.54 | -0.49 | 177.1 | 0.90 | 62.2 | -0.03 |
| 22 | 181 | 56 | 180.46 | -0.54 | 27.41 | -0.51 | 179.52 | 1.48 | 50.8 | -0.09 |
| 23 | 151 | 30 | 144.94 | -6.06 | 22.86 | -0.24 | 140.00 | 11.00 | 26.1 | -0.13 |
| 24 | 43 | 55 | 48.87 | 5.87 | 47.65 | -0.13 | 45.17 | 2.17 | 64.11 | 0.17 |
| 25 | 352 | 20 | 343.56 | -8.44 | 61.75 | 2.09 | 356.55 | 4.55 | 72.15 | 2.61 |

Systemic error is quite relevant to the type of data and the method used. Image resolution is the decisive factor in the analysis of a DEM and remote sensing images, which were provided by Google Earth in this study. Because Google Earth provides a massive database, we can choose the most appropriate images that were collected at the right time with good weather to use in this study; appropriate images display the target outcrop clearly (Zuo *et al*.,2008). In this paper, we used SPOT6, IKONOS, and QuickBird images in our analysis, with a resolution near to or less than 1 m.

In addition, Google Earth generates topography using a DEM with a spatial resolution of 30 m and a vertical accuracy of 16 m. Therefore, the DEM used here cannot express topography clearly in a flat field of view; attempts to do so will lead to a larger than average error in that situation. A previous study shows that the dip accuracy may be 1–4 °if the maximum horizontal separation ranged from 100–400 m; in addition, using DEM data with a low resolution may lead to a larger dip error (Berger *et al*.,1992; Duan *et al*.,2011). For this reason, that former study used stereo images to generate a DEM with the goal of improving the resolution of the DEM in that study (Chen et al., 2007).

Another systemic error is a result of the method used. We found the accuracies of our data were quite closely related to the continuity, fluctuations and morphological characteristics of the trace; we then summed the adaptive range for each method, while considering the geology and geomorphology of each site. Statistical analysis showed that the Multiple-point Method performed more poorly in both situations, especially for a discontinuous trace. The Multiple-line Method performed fairly well in most situations, but the results were a little disappointing in a flat field setting; this reflects the influence of the resolution of the DEM but not the disadvantages of this method. For the same reason, both methods cannot fit the plane well for a curved trace.

As the results show, the Multiple-line method is more accurate than the Multiple-point Method when both are compared with field data. However, we found the results of both methods deviate from the field data in some places, such as sites No. 14 and No. 25. We found an error for dip direction of about 25 °at Site No. 14, and an error of dip of about 45 °at No. 25. We collected all the field data by ourselves and feel confident in their reliability. Fortunately, we found that Site No. 14 was so close to No. 15 that they overlapped into one symbol (Fig. 3). After comparing the orientation of these two places and interpreting the results with data by both methods, we found that the orientation in Site No. 14 was slightly different from No. 15 in both dip direction and dip. We determined the dip direction at Site No. 14 was similar to No. 15; that is true because both the Multiple-line and Multiple-point methods measure the bedding orientation as a whole, which is an average on a small scale.

## 4 CONCLUSIONS

The measurement of bedding orientation based on remote sensing images provides a low-cost, rapid, and efficient method

that is useful for geologists, especially for challenging environments with low vegetation coverage and good bedding outcrops. The Multiple-point Method has been used traditionally in this field for many years, but will contain large errors for a discontinue outcrop. In this paper, we proposed a new method, the Multiple-line Method, with the goal of improving bedding orientation measurement in this field. We applied both the Multiple-line and Multiple-point method to Yili Basin, and compared the results with field data. The results show that both methods usually measure bedding orientation very well on a small scale; however, the Multiple-line Method has a wider range of application than the Multiple-point Method and yields more accurate results, especially in areas with flat fields and mountain ridges. The final publication is available at Springer via https://doi.org/10.1007/s12583-017-0943-1.

## ACKNOWLEDGMENTS

The authors would like to thank Li Li and Hao Liang for their help in field data measuring, and Ke Zhang and Shimin Wu for their guidance and support in structural geology. The work was in part supported by the National Natural Science Foundation of China (Nos. 41572316; 41102131), the Guangdong Natural Science Foundation (No. 2015A030313193).

## REFERENCES

Abellán, A., Vilaplana, J. M., Martínez, J., 2006. Application of a Long-Range Terrestrial Laser Scanner to a Detailed Rockfall Study at Vall de Núria (Eastern Pyrenees, Spain). *Engineering Geology*, 88(3/4):136–148. https://doi.org/10.1016/j.enggeo.2006.09.012

Bilotti, F., Shaw, J. H., and, 2000. Quantitative Structural Analysis with Stereoscopic Remote Sensing Imagery. *AAPG Bulletin*, 84(6): 727–740. https://doi.org/10.1306/a96733d8-1738-11d7-8645000102c1865d

Banerjee, S., Mitra, S., 2004. Remote Surface Mapping Using Orthophotos and Geologic Maps Draped over Digital Elevation Models: Application to the Sheep Mountain Anticline, Wyoming. *AAPG Bulletin*, 88(9): 1227–1237. https://doi.org/10.1306/02170403091

Berger, Z., 1993. Geologic Stereo Mapping of Geologic Structures with SPOT Satellite Data: REPLY. *AAPG Bulletin*, 76(1): 101–120. https://doi.org/10.1306/bdff8cea-1718-11d7-8645000102c1865d

Chen, J. P., Miao, F., 1991. The Calculating Method for Layer Attitude with Airphoto Pair. *Remote Sensing For Land & Resources*, 3(4): 40–45 (in Chinese with English Abstract)

Chen, N. H., Wang, X., Li, S.Q., 2009. Surface Deformation of the Middle Segment in the Qiulitag Belt of the Southern Tianshan Mountain, China: Remote Sensing-Aided Character Extraction. *Chinese Journal of Geology*, 44(3): 931–944 (in Chinese with English Abstract)

Chen, N., Wang, X., Yang, S., 2007. Quantitative Extraction of Shallow Stratum Information Based on CORONA Imagery. *Journal of Zhejiang University*, 41(4): 662–667 (in Chinese with English Abstract)

Duan, F. Z., Zhao, W. J., Li, J. C., et al., 2011. Measurement Method of Strata Attitude Based on Three-Dimensional Geographic Information System. *Journal of Jilin University* (*Earth Science Edition*), 41(10): 310–315 (in Chinese with English Abstract)

Dadon, A., Peeters, A., Ben-Dor, E., et al., 2011. A Semi-Automated GIS Model for Extracting Geological Structural Information from a Space-borne Thematic Image. *GIscience & Remote Sensing*, 48(2): 264–279. https://doi.org/10.2747/1548-1603.48.2.264

Dhont, D., Luxey, P., Chorowicz, J., 2005. 3-D Modeling of Geologic Maps from Surface Data. *AAPG Bulletin*, 89(11): 1465–1474. https://doi.org/10.1306/06270504108

Fernández, O., 2005. Obtaining a Best Fitting Plane through 3D Georeferenced Data. *Journal of Structural Geology*, 27(5): 855–858. https://doi.org/10.1016/j.jsg.2004.12.004

Fernandez, O., Jones, S., Armstrong, N., et al., 2008. Automated Tools within Workflows for 3D Structural Construction from Surface and Subsurface Data. *GeoInformatica*, 13(3): 291–304. https://doi.org/10.1007/s10707-008-0059-y

Grenon, M., Laflamme, A. J., 2011. Slope Orientation Assessment for Open-Pit Mines, Using GIS-Based Algorithms. *Computers & Geosciences*, 37(9): 1413–1424. https://doi.org/10.1016/j.cageo.2010.12.006

Guan, S. W., Wang, X., Yang, S. F., et al., 2003. 3-D Structural Analysis on the Kuqa's Qiulitag Anticline Zone of the Southern Tianshan Mountains, China. Geological Review, 49(5): 464–473 (in Chinese with English Abstract)

Jones, R. R., Kokkalas, S., McCaffrey, K. J. W., 2009. Quantitative Analysis and Visualization of Nonplanar Fault Surfaces Using Terrestrial Laser Scanning (LIDAR)——The Arkitsa Fault, Central Greece, as a Case Study. *Geosphere*, 5(6): 465–482. https://doi.org/10.1130/ges00216.1

Koike, K., Nagano, S., Kawaba, K., 1998. Construction and Analysis of Interpreted Fracture Planes through Combination of Satellite-Image Derived Lineaments and Digital Elevation Model Data. *Computers & Geosciences*. 24(6): 573–583. https://doi.org/10.1016/s0098-3004(98)00021-1

Liu, H., Ran, Y. K., Li, A., 2011. Attitude Extraction of Shallow Stratum Based on P5 Stereo Images and Geoeye-1 Image. *Seismology and Geology*, 33(4): 951–962 (in Chinese with English Abstract)

Pu, H., Yang, X. L., Zhao, H. F., et al., 2012. Measurement Method of Strata Attitude Based on Google Earth. *Journal of Southwest Jiaotong University*, 47(6): 949–954 (in Chinese with English Abstract)

Reif, D., Grasemann, B., Faber, R. H., 2011. Quantitative Structural Analysis Using Remote Sensing Data: Kurdistan, Northeast Iraq. *AAPG Bulletin*, 95(6): 941–956. https://doi.org/10.1306/11151010112

Tator, B, A., 1960. Photo Interpretation in Geology, Manual of Photographic Interpretation. American Society of Photogrammetry, Washington D. C. 169–343

Tan, J., Song, Y., 2011. Archives System of Remote Sensing Data Based on Google Earth. *Acta Geologica Sichuan*, 31(3): 364–368 (in Chinese with English Abstract)

Zhou, C., Zhu, H., Li, X., 2011. Research and Application of Robust Plane Fitting Algorithm with Ransac. *Computer Engineering and Applications*, 47(7): 177–179 (in Chinese with English Abstract)

Zuo, G. C., Zhang, Z. H., Wang, Z. L., et al., 2008. Tectonic Division, Stratigraphical Stystem and the Evolution of western Tianshan Mountains, Xinjiang. *Geological Review*, 54(6): 748–767 (in Chinese with English Abstract)